공학석사 학위논문

심혈관 중재시술을 위한 원격제어 로봇 시스템의 직관적 제어 구현 기법 연구

A study on the methods of intuitive control implementation in a teleoperation robot system for cardiovascular intervention

울산대학교 대학원

의 과 학 과

최 주 은

심혈관 중재시술을 위한 원격제어 로봇 시스템의 직관적 제어 구현 기법 연구

지 도 교 수 최 재 순

이 논문을 공학석사학위 논문으로 제출함

2022 년 2 월

울산대학교 대학원
의 과 학 과
최 주 은

최주은의 공학석사학위 논문을 인준함

심사위원 김 준 기 (인)

심사위원 최 재 순 (인)

심사위원 문 영 진 (인)

울 산 대 학 교 대 학 원

2022 년 2 월

ABSTRACT

Cardiovascular intervention is widely used for treating cardiovascular disease. X-ray exposure during operation, fatigue due to long-time operation, and experience-dependent successful rate are serious problems for physicians in the intervention procedures.

This study proposed in a developed robotic system using roller modules for cardiovascular intervention and the methods of intuitive control of the system. The slave robot can control the vascular instruments such as a guiding catheter, guidewire, and balloon/stent catheter by commands from the physician who is manipulating the master haptic interface.

The roller-cartridge-based modularized robotic system in the slave robot is designed to have advantages such as active clamping of various vascular instruments and the capability of individually or simultaneously inserting and rotating them. A compensation method using experimental results was adopted for solving errors or tolerances that occur while configuring the roller cartridge as a detachable sterilized product in consideration of clinical practicality. The study also proposed several haptic rendering functions of the master haptic interface for convenient operation of physicians.

The basic performance associated with positioning accuracy and precision in translational and rotational motions of vascular instruments using the robotic system was tested. The results showed sufficiently high accuracy and precision for application in the intervention procedure. The accuracy of the translational and rotational motion of them were within 1 mm and 5°, respectively. It was also confirmed through animal and clinical trials that the system demonstrates good performance and can safely be applied clinically to patients with heart diseases.

Key word: **Cardiovascular intervention, Medical robot, Teleoperation control, Master-slave system, Guidewire**

TABLE OF CONTENTS

LIST OF FIGURES

LIST OF TABLES

INTRODUCTION

1. Background

1.1. Percutaneous coronary intervention (PCI)

Cardiovascular intervention is to treat cardiovascular disease in minimally invasive manner, and the application area has been rapidly extended with advantages over conventional surgical methods. Especially, percutaneous coronary intervention (PCI) refers to a family of minimally invasive procedures used to open clogged coronary arteries (those that deliver blood to the heart). Prior to the advent of PCI, patients with multivessel coronary artery disease had to undergo open heart surgery. In a PCI, the doctor reaches a blocked vessel by making a small incision in the wrist or upper leg and then threading a catheter (a thin, flexible tube) through an artery that leads to the heart. The doctor uses X-ray images of the heart as a guide to locate the blockage or narrowed area, and then uses the most appropriate PCI techniques to open the vessel. PCI can improve symptoms of blocked arteries, such as chest pain or shortness of breath by restoring blood flow.

PCI procedures proceeds as follows. First, a guide catheter is inserted into the femoral artery at the groin or the radial artery at the wrist of the patient to the opening of the affected coronary artery. Next, a guidewire is inserted into the guide catheter and navigated past the obstructed area (“lesion”) in the coronary arteries in Figure 1. A balloon catheter is then introduced into the body and maneuvered over the guidewire to the lesion. The balloon is inflated to push the plaque against the artery wall to expand the arterial lumen in Figure 1[1)].

However, the procedure has unavoidable dependence on fluoroscopy or angiography system[2-3)], and the clinical outcome and the complication rate vary widely among physicians with different experience levels. Long flexible instruments such as catheters or guidewires inserted through a vessel with blood flow around it demonstrates nonlinearity and complexity in controlling the motion and requires long-term training of physicians with a stiff learning curve. Even experienced physicians may need a considerably long time to perform the procedure

depending on the type of procedure[4-5]. Robotic systems to assist cardiovascular intervention procedures have been developed. The robotic systems' primary advantage is the reduction of radiation exposure by the teleoperation configuration[6-8]. Additional advantages may include increased precision, accuracy, and ease of motion of vascular instruments. Numerous research groups are continuously presenting new research and development attempts, and the interest of physicians in robotics technologies has been significantly increasing.

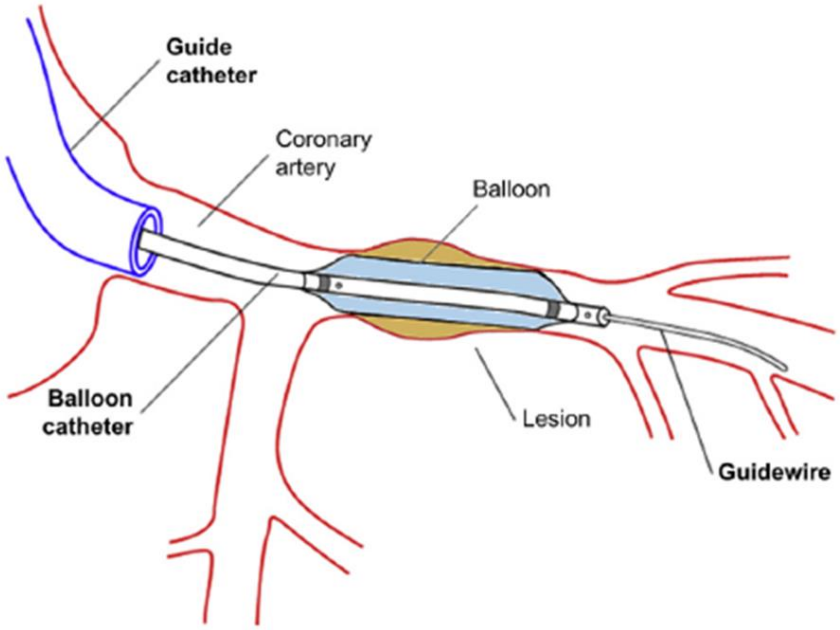

Figure 1. Schematic diagram of a lesion in the coronary, and the use of the guide catheter, balloon catheter, and guidewire in treating diseased coronary artery[1].

1.2. Robot-assisted Percutaneous coronary intervention (R-PCI)

The problems from PCI procedure were described in chapter 1.1. Robotic-assisted PCI involves remote navigation of devices inside the patient's body. As shown in Figure 2, during the robot-assisted vascular intervention surgery, physicians operate a haptic interface in the master console, which is located at a safe distance from the ionizing radiation source, to control a slave end-effector tasked with advancing, retracting, and rotating vascular instruments under the guidance of a real-time fluoroscopic image[9-10].

Being seated at a master console negates the need for wearing heavy leaded aprons and may reduce musculoskeletal strain. Clinical studies have shown that physicians performing robotic-assisted PCI are exposed to significantly less scatter radiation than clinicians at the bedside[11, 12]. Some studies on robotic-assisted PCI have shown a trend toward reduced fluoroscopy time and less use of contrast media[12, 13]. This may relate to the enhanced visualization offered by being seated near high-definition monitors in the master side.

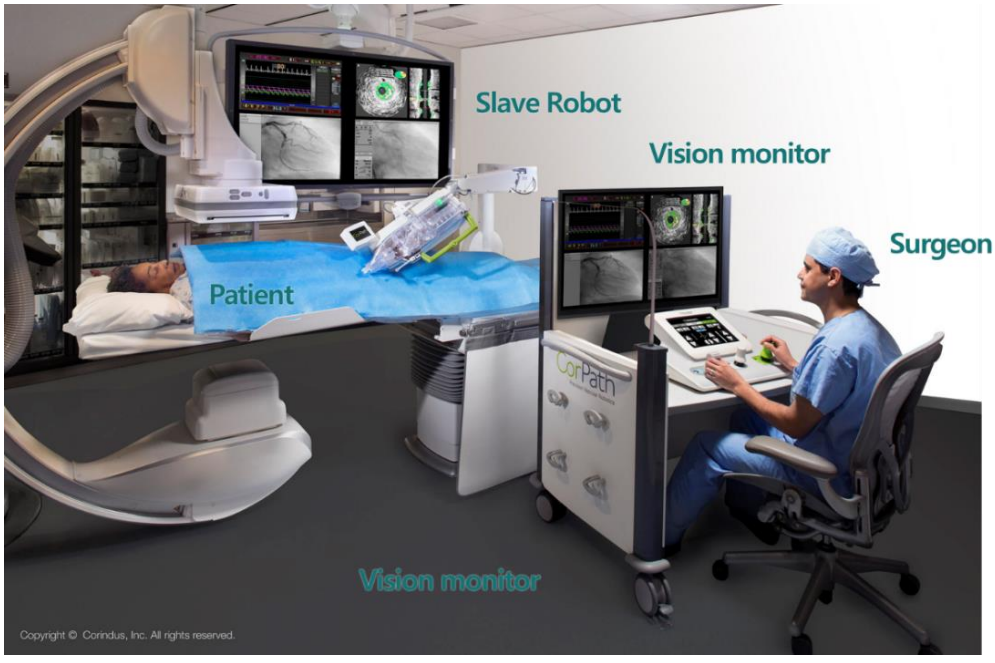

Figure 2. Master-slave teleoperation system (Images: CorPath system ©2016 Corindus Inc.).

1.3. Related works

Researchers have designed various robotic systems for PCI. Mahmud et al.[14] provided a good review on robotic technology in interventional cardiology. Commercial products including Magellan™ (Hansen Medical, Mountain View, CA)[15-17] and CorPath® (Siemens Healthineers, Erlangen, Germany)[18] have received approvals from the United States Food and Drug Administration. The Magellan™ Robotic System controls a specially designed robotic catheter which is composed of a leader and a sheath and deflected by tendon, and has the master console which has a control panel and a commercial 6 DOF (degrees of freedom) master device, produced by Force dimension, and controls the robotic system. However, Magellan only uses their specific catheters and guidewires, so it is difficult to apply various types of surgical tools in Magellan system.

The CorPath is a practical robotic system by employing a commercial guidewire and balloon catheter. It controls insertion and rotation of a guidewire and the stent insertion. The robot is controlled by a control console which has two joysticks and a touch screen panel. However, the diameter of the catheters that can be used in CorPath series robots is fixed[14]. The CorPath series robots are only compatible with 0.14-inch guidewires and rapid exchange balloons and stents. Furthermore, neither of the above solutions include haptic or force feedback functions in the master device of the teleoperation system[19].

In the research domain, Thakur et al.[20-21] presented a master-slave catheter navigation system that a surgeon manipulates commercial catheter mounted on the master site with two degrees of freedom (DOF), that is, translational and rotational motions. The position information of the catheter at the master device are sensed. A slip-ring gantry of the slave robot holds and guides the catheter and the catheter is controlled by an axial driving mechanism mounted in a slip-ring gantry. Cha et al.[22] have also developed a robotic system designed explicitly for interventional radiology procedures such as Transcatheter Arterial Chemo-Embolization, which may have limitations in cardiovascular procedure application.

2. Objectives

Commercial robotic systems have no force feedback function and control a few sizes of vascular instruments. In this study, a design of a robotic vascular intervention system with active clamping mechanism was proposed. It enables quick setting and retrieval of the vascular instruments in an emergency response situation. The active clamping mechanism allows the use of various vascular instruments with different diameters and internal structures, such as guiding catheter extension and intra-vascular ultrasound (IVUS) catheters.

The methods of intuitive control implementation in the proposed system were presented. A compensation method using experimental results was adopted for solving errors or tolerances that occur while configuring the roller cartridge as a detachable sterilized product in consideration of clinical practicality. The study also proposed several haptic rendering functions of the master haptic interface for convenient operation of physicians. Finally, to verify the functionality and safety of the proposed system, the proposed robotic system is evaluated through phantom experiment, in-vivo test and clinical trial.

The remainder of this study is organized as follows: designs of the robotic system including the mechanism design, a direct kinematic analysis are described in Method section 1. Methods of controlling the vascular instruments precisely in the roller module, controlling master-slave system such as motion mapping, and compensation methods are described in Method section 2.

The evaluation experiments and the results obtained by the robotic system including the compensation evaluation, evaluation of motion of the vascular instruments, in-vivo test, and the clinical trial are described in Experiment and Result Section. Discussions and conclusions are presented.

METHOD

1. System Description

1.1. Overview of Slave End-effector

1.1.1. Concept of Slave End-effector

The end-effector of the slave-side system features a set of roller cartridges that can perform both translation and rotation and accommodate instruments with various diameters by an active clamping mechanism in one unified unit for modular configuration[23].

As shown in Figure 3, the translation mechanism advances or retracts vascular instruments by axially rotating the tightly pressed roller pairs. The rotation mechanism rotates vascular instruments by rubbing the roller pair. The roller mechanism was chosen for uninterrupted translational motion control of the vascular instruments[24–26].

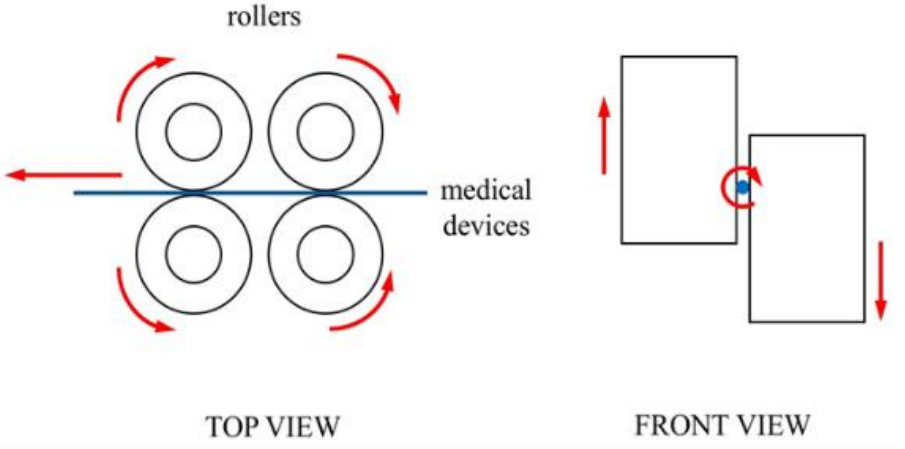

Figure 3. Concept of the Roller system for translational and rotational motions of vascular instruments.

1.1.2. Design of Slave End-effector

Based on the concepts, the end-effector in the slave robot shown in Figure 4 (a) consists of three modules for three types of instruments, a y-connector supporter, and tool supporters. Three modules are used to separately actuate a guiding catheter, guidewire, and balloon/stent catheter. The guiding catheter and guidewire module are 3-DOF roller systems that clamp,

translate, and rotate a target instrument in Figure 4 (b) ~ (d). The balloon/stent module is a 2-DOF roller system identical to the other modules but does not have a rotation function. The guidewire and balloon catheter modules are mounted on a movable base plate in order to maintain the distance to the catheter module, depending on the guiding catheter's translation.

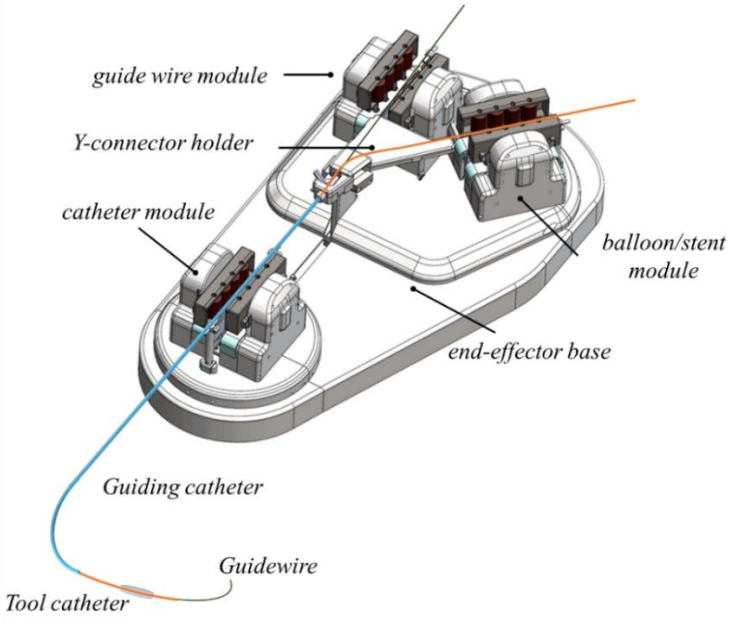

(a)

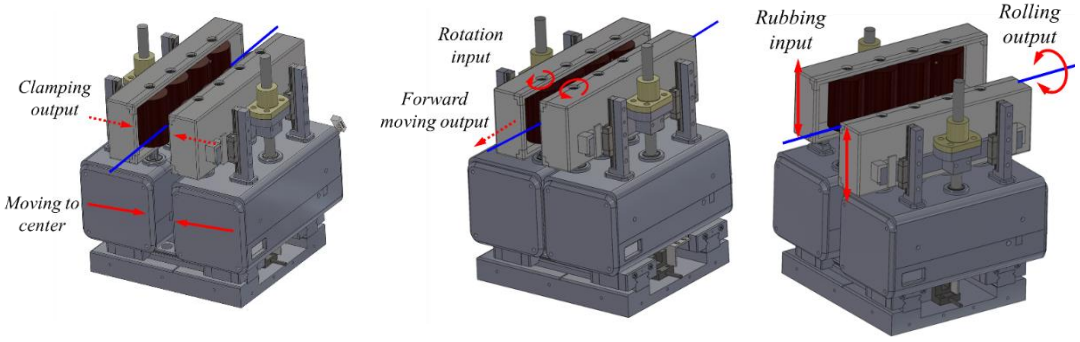

(b) (c) (d)

Figure 4. Design of the slave end-effector.

(a) The slave end-effector and the motion principles of (b) clamping mechanism, (c) translation mechanism, and (d) rotation mechanism in the roller module.

1.2. Overview of Master Haptic Interface

1.2.1. Design of Master Haptic Interface

The master haptic interface[23], which is an improvement of a design presented in a previous study[27], has been designed as shown in Figure 5 (a). A planar mechanism is attached to a moving block under the linear actuator, and the spherical mechanism is attached to the top of the linear actuator. The spherical mechanism captures the wrist rotation movement of the physician holding the grip, which corresponds to the rotational motion of the vascular instrument, as shown in Figure 5 (b). The planar mechanism is a widely known 3-RRR-type parallel mechanism[28–30]. It consists of a planar orthogonal motion of two DOFs and a vertical axis rotational motion, allowing a 3-DOF movement. While the physician moves the moving platform on the planar mechanism, the forward and backward translational movement is captured and corresponded to the vascular instruments' translational motion, as shown in Figure 5 (c). The linear actuator between the two mechanisms acts as a clutch-like trigger for the movement of the tools. When the physician presses the spherical mechanism downward through the linear actuator, the master–slave teleoperation is connected, and the slave robot motion is locked when released.

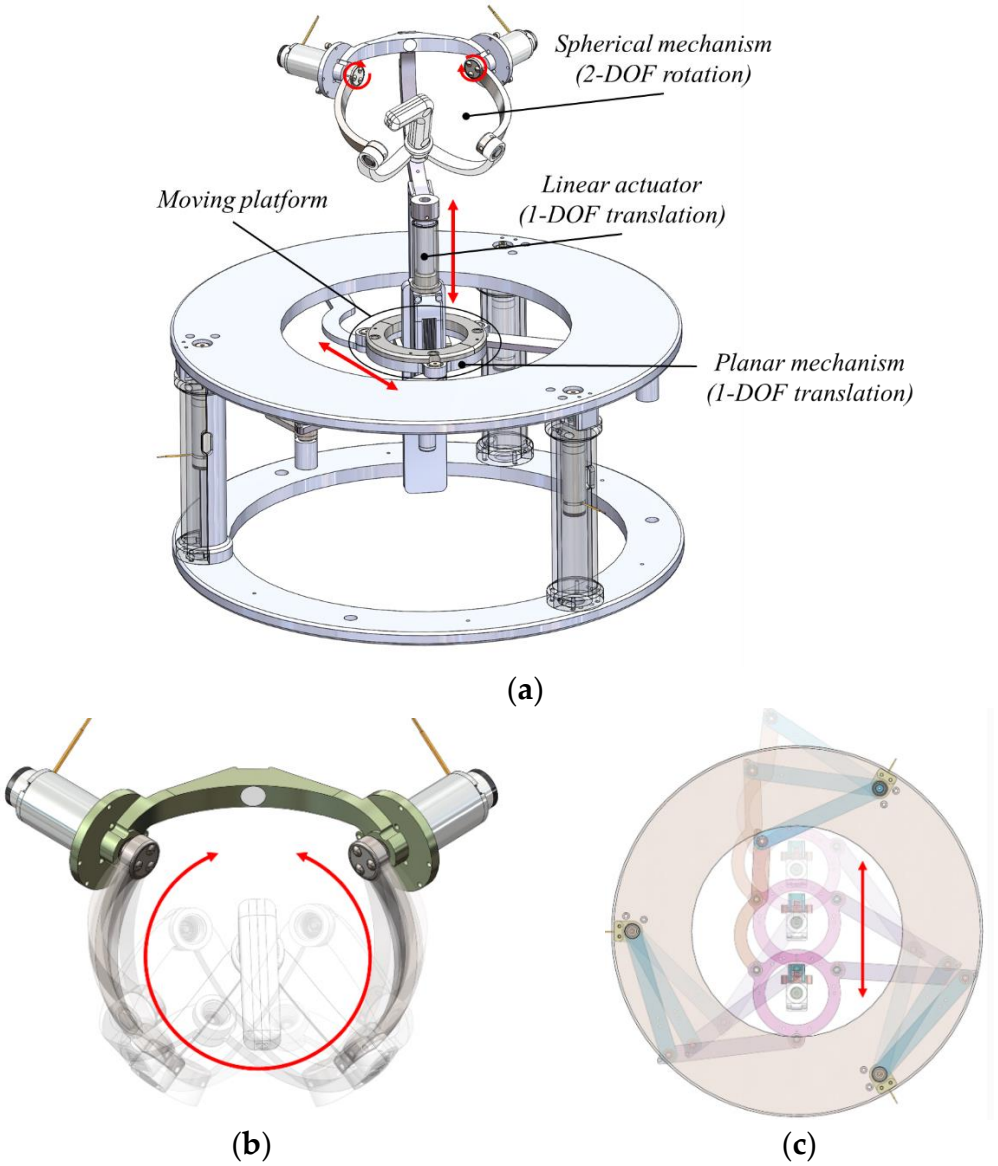

Figure 5. Design of the master haptic interface.

(a) Design of the master haptic interface. Master haptic interface matching concept of (b) rotational motion, and (c) translational motion.

1.2.2. Inverse Kinematics of the master haptic interface

To implement haptic functions in the master interface, the inverse kinematic of the master haptic interface is calculated. The kinematic structure of the master haptic interface in Figure 6.

The inverse kinematic of the 3-RRR parallel mechanism[31] is to find the input joint angles, θ_i, for $i = 1, 2,$ and 3, for a given moving platform position, $p = [x,\ y,\ \varphi]$ as shown in Figure 6 (a). From mechanism's geometry and from the closure equation as follows:

$$OP = \overline{OA_i} + \overline{A_iB_i} + \overline{B_iC_i} + \overline{C_iP} \tag{1}$$

$$P_x = l_{Ai}cos(\theta_i) + l_{Bi}cos(\psi_i) + l_{di}cos(\sigma_i + \varphi) + A_{xi}$$
$$P_y = l_{Ai}sin(\theta_i) + l_{Bi}sin(\psi_i) + l_{di}sin(\sigma_i + \varphi) + A_{yi} \tag{2}$$

where σ_i is the angle between the lines from the point P to the line between C_1 and C_2 on the moving platform.

So, θ_i are found as follows:

$$\theta_i = A\,tan\,2(K_i, F_i) \pm A\,tan\,2\left(\sqrt{\left(K_i^2 + F_i^2 - E_i^2\right)}, E_i\right), (i = 1, 2, 3) \tag{3}$$

Where:

$$E_i = P_x^2 + P_y^2 + L_{A_i}^2 - L_{B_i}^2 + L_{c_i}^2 + A_{x_i}^2 + A_{y_i}^2$$
$$-2P_x l_{c_i}\cos(\sigma_i + \varphi) - 2P_x A_{xi} + 2l_{ci}A_{xi}\cos(\sigma_i + \varphi)$$
$$-2P_y l_{ci}\sin(\sigma_i + \varphi) - 2P_y A_{yi} + 2l_{ci}A_{yi}\sin(\sigma_i + \varphi)$$
$$F_i = 2P_x l_{Ai} - 2l_{Ai}l_{ci}\cos(\sigma_i + \varphi) - 2l_{Ai}x_{Ai}$$
$$K_i = 2P_y l_{Ai} - 2l_{AI}l_{ci}\sin(\sigma_i + \varphi) - 2l_{Ai}y_{Ai}$$

The inverse kinematic of the spherical mechanism is solved to determine the angular displacements of each motor on the mechanism for the given coordinate of E. $\overline{AO}$, $\overline{BO}$, $\overline{CO}$, $\overline{DO}$, and $\overline{EO}$ intersect at a common point O. $\overline{DO}$ is in the x–z plane and $\overline{CO}$ is in the y–z plane. Therefore, two angles are defined as θ_1 and θ_2, as shown in Figure 6 (b). For the

position of the E set as $[x, y, z]^T$ in Figure 6 (b), the vector of the grip is determined as follows:

$$\overline{OE'} = \begin{bmatrix} tan(\theta_2)z \\ tan(\theta_1)z \end{bmatrix}, \tag{4}$$

$$\theta_1 = ATAN2(y, z)\left(\frac{\pi}{2}\theta_1 < \frac{3\pi}{2}\right), \theta_2 = ATAN2(x, z)\left(\frac{\pi}{2}\theta_2 < \frac{3\pi}{2}\right) \tag{5}$$

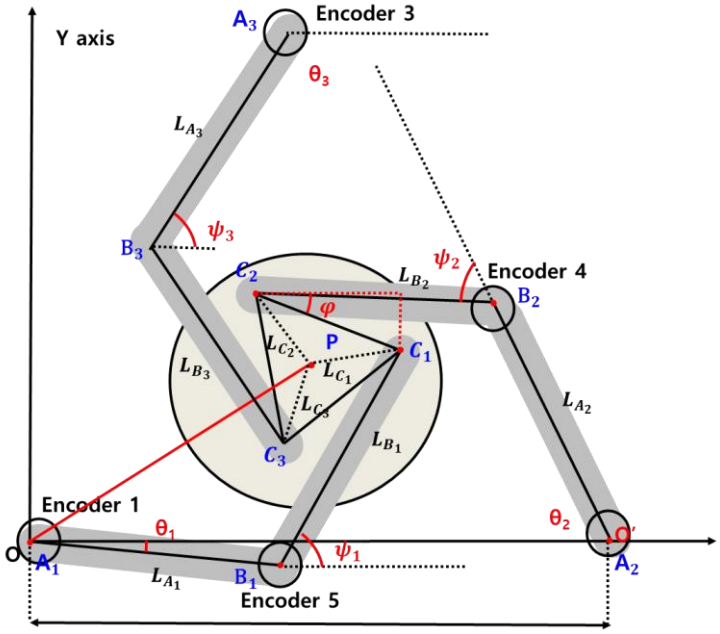

(a)

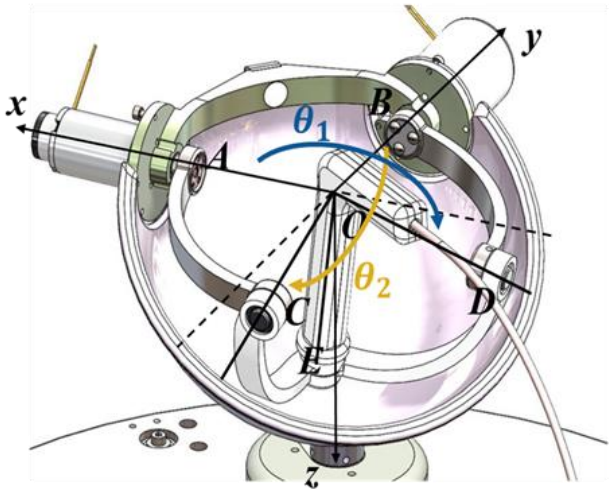

(b)

Figure 6. Geometric structure of the master haptic interface

(a) the 3-RRR parallel mechanism. (b) the spherical mechanism.

2. Master-Slave system

2.1. Control System

Figure. 7 shows the prototype of the master-slave system. Most parts of the prototype, excluding certain metal components and the motors, are manufactured from polyester ether ketone. A master console predominantly consists of a haptic interface, two touch panels, a master base, and display monitors. Physicians can select the type, size and speed of the vascular instruments by pushing buttons in the touch panel. In addition, through the display touch panel, physicians monitor the motion of the end-effector, such as displacement in translational motion and angle in rotational motion. The display monitors show the real-time fluoroscopy image.

A communication diagram of the master-slave system is shown in Figure. 8. Physicians operate the master haptic interface on the master console to control the slave end-effector for performing the surgery. At the same time, physicians can monitor the fluoroscopy image through the display monitor in real-time to obtain visual feedback. The master haptic interface and slave end-effector are actuated using DC motors (Maxon Motor Inc., Switzerland), which are controlled by PCs and motor drivers in the base of the consoles.

The motor controllers are connected to the PC by a controller area network bus set at 500 Hz. The control software was developed in C++, and the graphic user interface on the touch panels was developed using Qt software (The Qt Company, USA). The communication frequency of the user datagram between the master and slave control systems is 500 Hz.

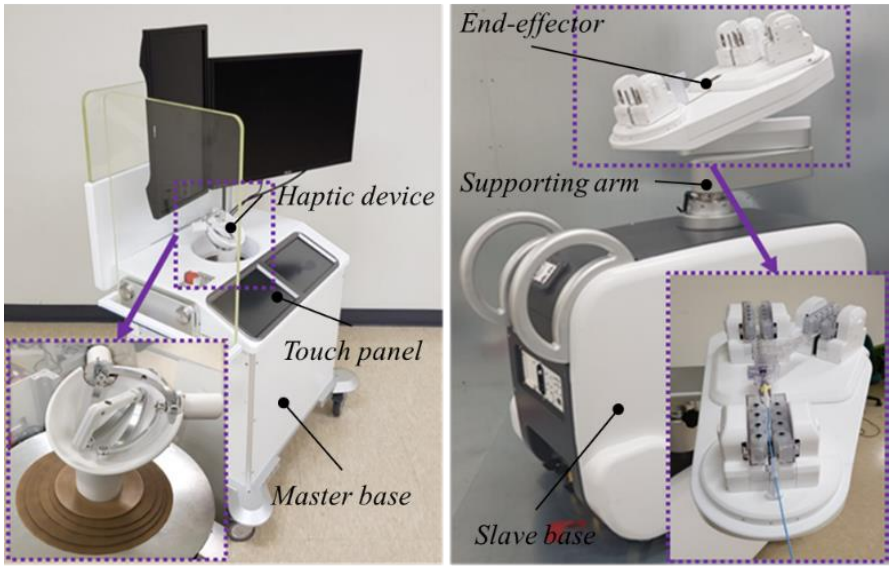

Figure 7. Clinical prototype of the master-slave robotic system.

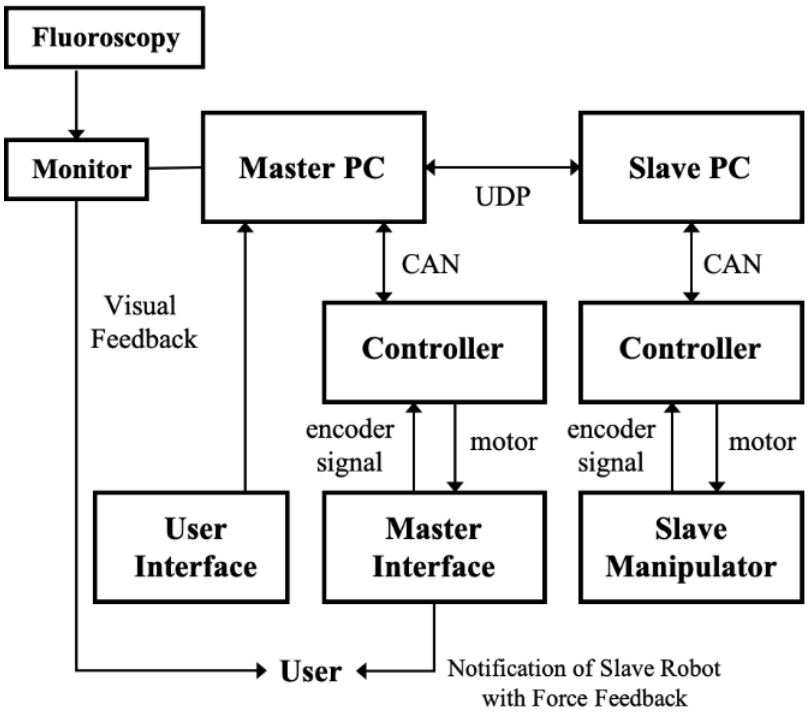

Figure 8. Communication diagram of the master–slave robotic system.

2.2. Motion Model of Vascular instruments

The output angle of the motors for translation or rotation can be measured by the encoder installed at the end of each motor. According to the mechanical structure and dimension of the roller system, the relationships between the axial displacement of vascular instruments and output angle of the translation motor, and the rotation angle of the vascular instruments and output angle of the rotation motor can be calculated.

1. Clamping motion model: It should be ensured that the vascular instruments are reliably clamped by the two roller cartridges, and they do not slip during rotation and translation. The clamping force is determined by the static torque of the clamping motor. Therefore, during model selection of the clamping motor, the static torque of motor is a key consideration.

2. Translational motion model: The output angle of the translation motor θ_{TR} (rad) and axial displacement of vascular instruments, s (mm), satisfies the following relationship.

$$s = g_T \times r \times \theta_{TR} \tag{6}$$

where g_T and r (mm) denote the ratio of the bevel gears and radius of the roller, respectively.

3. Rotational motion model: The output angle of the rotation motor and the upward or downward displacement of the roller modules are θ_{RO} (rad) and y_{rm} (mm), respectively. Then, the rotation angle of the vascular instrument, θ_t (rad), can be obtained by the following:

$$\theta_t = \frac{y_{rm}}{r_t} = \frac{g_R \times t \times \theta_{RO}}{r_t} \tag{7}$$

where r_t (mm) denotes the radius of the vascular instruments. g_R and t denote the ratio of bevel gears and ball screw pitch for the elevation of the roller cartridge, respectively.

2.3. Compensation Method

2.3.1. Compensation for Gap of Roller cartridge

As shown in Figure 9 (a), the gap in the holder is inevitable because the design has a minimal tolerance for assembling and disassembling the disposable roller cartridge from the bar of the roller system. The gap of the roller cartridge is approximately 1 mm. Figure 9 (b) shows an example of backlash in the cartridge's vertical movement.

Due to this backlash, physicians experience a certain amount of delay in rotational motion when the direction of the motion changes. An experimentally obtained compensation value was used to a resolve the delay.

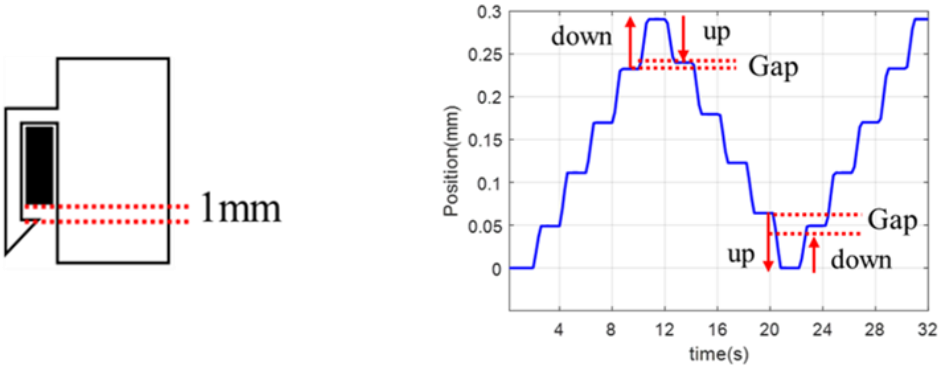

(**a**) (**b**)

Figure 9. Characteristics of the roller cartridge. (a) Gap between the roller cartridge and the bar of the roller module. (b) Position of the roller cartridge by pre-compensated control.

2.3.2. Haptic Rendering for Rotation Notification

The rotational motion has a limited range due to the limited height of the roller cartridge. The vertical displacement of the roller cartridge during the rotational motion is 25 mm, and the maximum degree of rotation can be between approximately 900° and 1,800°, depending on the vascular instrument's diameter. This appears to be sufficient to rotate the vascular instruments required during surgery.

For the physician to recognize the rotational motion limit, haptic feedback of the repulsing force is rendered on the master grip when the roller cartridge in the slave end-effector approaches the limit. The haptic feedback is implemented as follows. First, the range of cartridges is set for haptic feedback. As shown in Figure 10 (a), the difference in height between the two cartridges is set as δ (mm). Then, the movement is performed with the motor's current control in the spinal mechanical part of the spherical mechanism of the master haptic interface, and the force and direction provided to the physician are determined. Next, we determine the amount of force for the haptic feedback according to the roller cartridge range. The current exerted at the position of the roller cartridge, δ, is calculated according to (8). The current drawn is directly proportional to the torque developed by the motor.

$$I_{hf1,\ 2} = \begin{cases} a \cdot \delta + b & (\delta_{min} \le |\delta| \le \delta_{max}) \\ 0 & (0 \le |\delta| < \delta_{max}) \end{cases} \tag{8}$$

where I_{hf1} is the current for the rotation motor on the right of the grip of the master haptic interface and I_{hf2} is the current for the rotation motor on the left.

By using the angles calculated by (5), the slope and y-intercept of the linear function are calculated by (9). The value of each parameter is as follows:

$$a = sgn \cdot \frac{I_{max} - I_{min}}{\delta_{max} - \delta_{min}},\ b = -a \cdot \delta_{min}$$
$$sgn = \begin{cases} +1 & (\theta_{1,\ 2\ current} - \theta_{1,2\ prev} \ge 0) \\ -1 & (\theta_{1,2\ current} - \theta_{1,2\ prev} < 0) \end{cases} \tag{9}$$

where $\theta_{1,\ current}$ and $\theta_{2,\ current}$ indicate the angles at the current status, and $\theta_{1,\ prev}$ and $\theta_{2,\ prev}$ indicate the angles at the previous status.

2.3.3. Haptic Rendering for Input of Master Haptic Interface

Haptic rendering of the base of the master haptic interface is implemented to create a virtual wall to help the physician move the handle in y-direction for translation command as shown in Figure 11.

If the moving platform is between the left and right virtual walls, there is no haptic, so the moving platform is moved freely. If the moving platform is inside the virtual walls, the force feedback from the motor is exerted to return the moving platform to its position between the virtual walls.

The force is proportional to the displacement of the moving platform, as it is shown in (10).

$$f_{wall} = \begin{cases} K(x_{mp} - x_{wall}) & if\ x_{mp} \geq x_{wall} \\ 0 & if\ x_{mp} < x_{wall} \end{cases} \quad (10)$$

where f_{wall} represents the reaction force exerted in the virtual wall, x_{mp} represents the displacement between origin and current position of the moving platform in x-direction and K the stiffness of the virtual wall. x_{wall} is the position of the wall in x-direction.

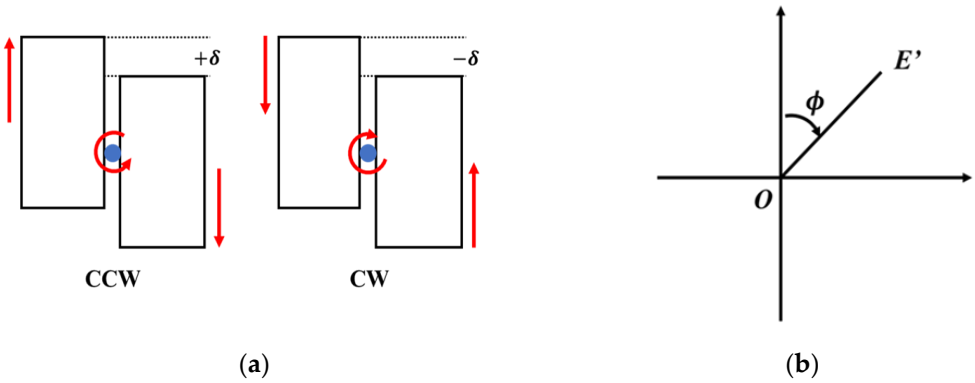

(**a**) (**b**)

Figure 10. Concept of rotation notification. (a) Roller cassettes depending on rotational direction. (b) Top view (projection on x–-y plane) of the master grip.

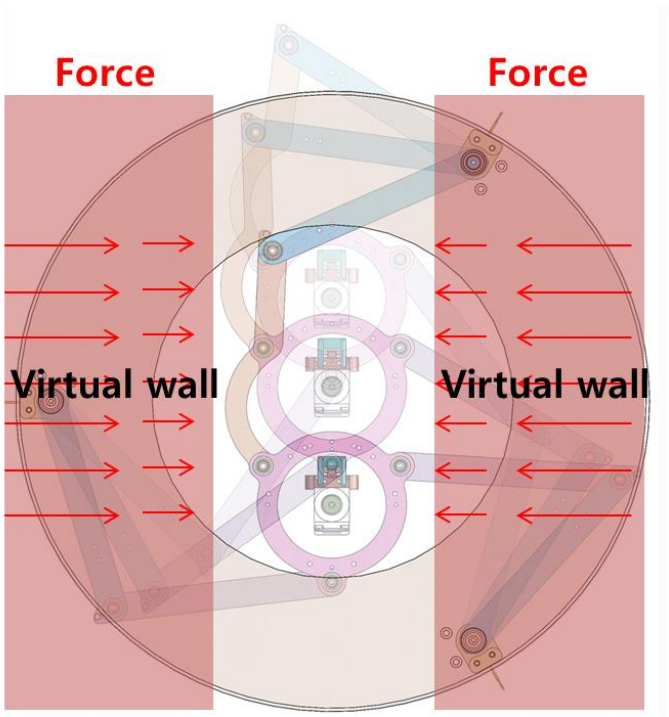

Figure 11. Concept of haptic rendering of the base of the master haptic interface.

EXPERMENTS AND RESULT

Experiments were conducted to evaluate the accuracy and precision of the vascular instruments' motion when operating the system, and to assess the robot-assisted intervention's effectiveness.

1. Compensation Evaluation

1.1. Evaluation for Gap of Roller cartridge

a) *Experimental Method:* A laser sensor (HL-G103-S-J, Panasonic, Japan) was placed vertically on the cartridge, and the vertical displacement of the roller cartridge was measured. An incremental command allows it to move up or down at regular intervals of 0.06 mm, which is the amount required for a 10° rotation of the guidewire. One trial included five increments of descending, ascending, and descending, and a total of 20 trials were performed. The displacement loss value was obtained through the 20 initial experiments without a compensation control. Then, the trials with a compensation control were repeated, changing the rotational direction.

b) *Experimental Results:* Figure 12 (a) shows that the proposed compensation method improved the backlash in the roller cartridge's vertical motion. The accuracy of the system was quantified by measuring the theoretical displacements and the averaged displacements with/without compensation in every trial, and calculating the root mean square error (RMSE). The RMSEs of the displacement with/without the compensation method were 0.0022 mm and 0.0055 mm, respectively. The system was able to follow the desired displacement accurately, reducing the RMSE by 40%.

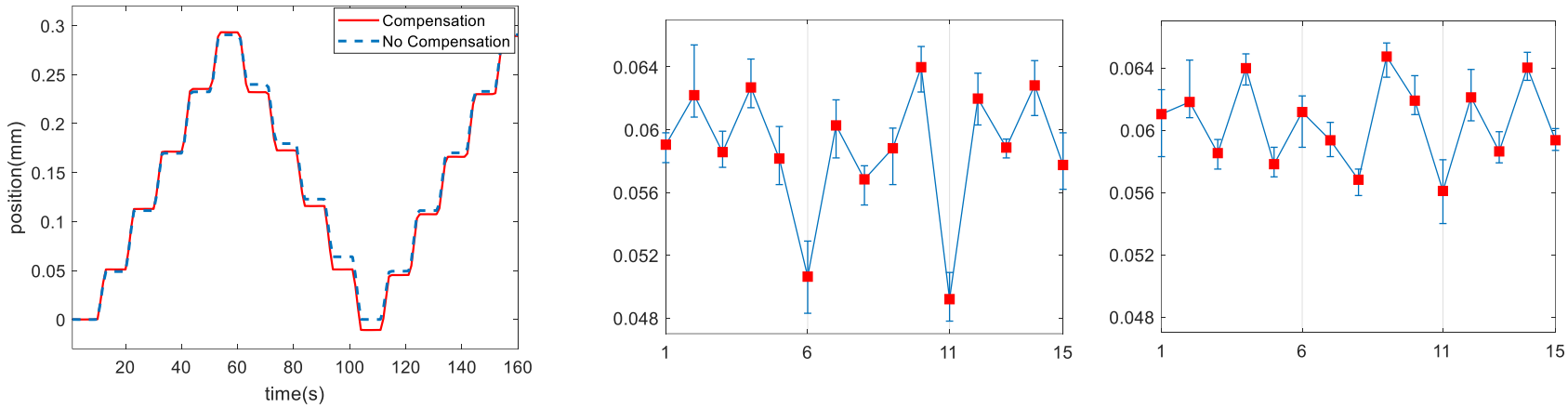

(**a**) (**b**) (**c**)

Figure 12. Result of the compensation of the gap of the roller cartridge. (a) Position of the roller cartridge from the laser sensor with/without compensation. (b) Without compensation. (c) With compensation; the data include the median and range of measured errors for 20 trials.

1.2. Evaluation for Rotation Notification

a) *Experimental Method:* When an operator first rotates the grip of the master haptic interface in the clockwise direction from the initial position for feedback ($-\delta_{min}$), -6.325 mm, to the maximum direction ($-\delta_{max}$), -6.5 mm, of the roller cartridge, we checked whether the torque value of the motors depends on θ_1, θ_2, and the position of the roller cartridge, (8) to (9). The two DC motors of the grip have a maximum power of 24 W and maximum continuous torque of 15.3 mNm. Moreover, the torque constant (K_t) is 18.4 mNm/A. When the physician operator rotated the grip in the opposite direction, from the initial position for feedback (δ_{min}) of 6.325 mm to the maximum direction (δ_{max}) of 6.5 mm of the roller cartridge, the torques were checked.

b) Experimental Results: Figure 13 illustrates the torques for haptic feedback depending on the directions of θ_1 and θ_2, and the position of the roller cartridge. When the displacement of the roller cartridge reached from -6.325 to -6.5 mm, the torque of the left motor for θ_1 increased linearly and that of the right motor decreased linearly, and the torques of the left and right motors were 15.364 and -15.364 mNm, respectively, at -6.5 mm for the clockwise rotation. Conversely, when the displacement of the roller cartridge reached from 6.325 to 6.5 mm, the torques of the left motor decreased linearly and that of the right motor increased linearly, and the torques of the left and right motors were -15.364 and 15.364 mNm, respectively, at -6.5 mm for clockwise rotation.

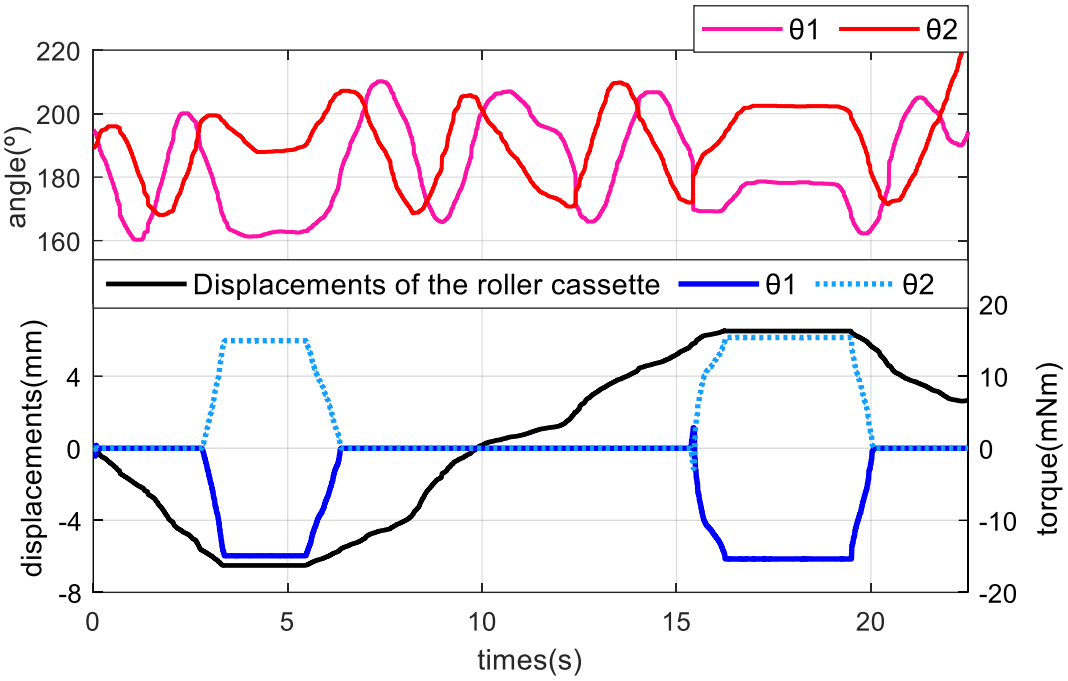

Figure 13. Torques for the haptic feedback depending on the directions of θ_1, θ_2, and the position of the roller cartridge.

2. Evaluation of Motion of Vascular instruments

a) Experimental Method: We conducted a series of experiments to characterize the accuracy and precision of the modularized system with an active clamping mechanism in the axial and radial directions. The experiment was set up as shown in Figure 14. The vascular instruments used in the experiment were a 5-F catheter, 0.014-inch guidewire, and a balloon catheter (3.5 × 15 mm). The actual displacement and angle of the vascular instruments were measured by using an electromagnetic (EM) tracking sensor with six DOFs (Aurora system, Northern Digital Inc., Canada). The accuracy was evaluated in terms of the absolute error (between the actual displacement/angle of the vascular instruments and the theoretical displacement). The axial and radial precision was evaluated by calculating the standard deviation of the absolute error. The accuracy and precision in translation were evaluated while the vascular instruments were placed in a 5 mm diameter vascular 2D path model produced by 3D printing, which was used to avoid introducing measurement error owing to the elastic deformation of the vascular instruments. To evaluate the accuracy and precision, the vascular instruments were advanced from 0 to 10, 20, 30, 40, and 50 mm, ten times in succession. An EM sensor was attached at the distal end of the vascular instruments and the spatial coordinates could be provided by the EM tracking system. The actual displacement of the catheter can be calculated by the following:

$$S_{act} = \sqrt{(x_2 - x_1)^2 + (y_2 - y_1)^2 + (z_2 - z_1)^2} \tag{7}$$

where (x_1, y_1, z_1) is the coordinate of the start point, and (x_2, y_2, z_2) is the coordinate of the end point.

b) Experimental Results: As a result, the accuracy (mean error) and precision (standard deviation) of the vascular instruments in translation are listed in Table I. It lists the average values of the vascular instruments for 10 trials. The mean errors of the motions of the roller module in the axial direction were within 1 mm for all the endovascular tools in each condition. The comparison of the accuracy and precision between the actual rotation angle and 360° are listed in Table II.

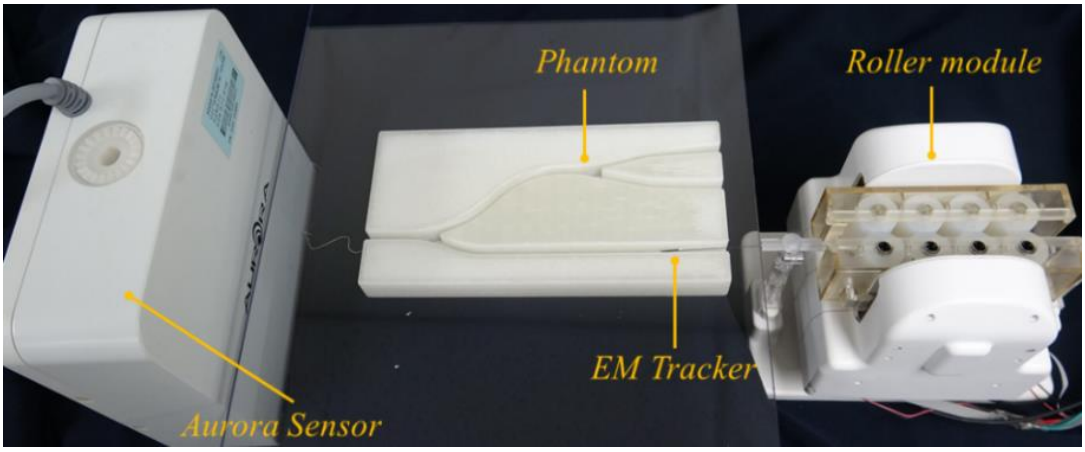

(a)

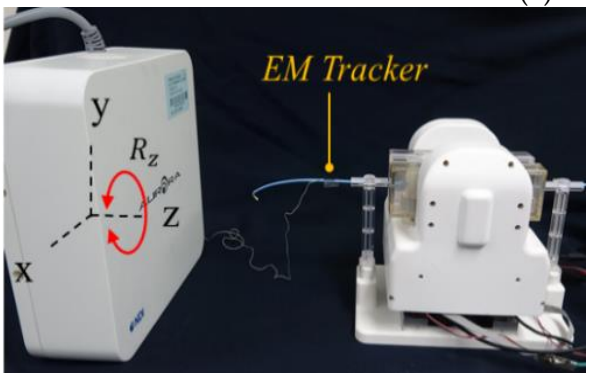

(b)

(c)

Figure 14. Setup for accuracy test of the motion of vascular instruments.

(a) translational motion, (b) rotational motion, (c) rotational motion in the front view.

Table 1. Accuracy and precision of translational motion of vascular instruments.

Tool	Theoretical Displacement (mm)	Averaged Actual Displacement (mm)	Mean Error (mm)	Standard Deviation (mm)
Guiding Catheter	10	9.38	–0.623	0.882
	20	19.54	–0.46	0.987
	30	29.01	–0.736	1.024
	40	39.07	–0.93	0.43
	50	50.75	0.75	0.12
Guidewire	10	10.71	0.71	0.39
	20	20.64	0.64	0.63
	30	29.9	0.11	0.54
	40	40.86	0.86	0.74
	50	50.24	0.24	0.74
Balloon Catheter	10	10.31	0.31	0.04
	20	20.07	0.07	0.03
	30	30.11	0.11	0.08
	40	40.57	0.57	0.42
	50	50.13	0.13	0.37

Table 2. Accuracy and precision of rotational motion of vascular instruments.

Tool	Theoretical Angle (°)	Averaged Actual Angle (°)	Mean Error (°)	Standard Deviation (°)
Guiding Catheter	360	363.29	3.29	5.48
Guidewire	360	361.93	1.93	2.50

3. Evaluation of Master-Slave Robotic System

3.1. Phantom test

a) Experimental Method: To test the transmission accuracy of a guidewire and balloon catheter, the experiment was conducted on a silicon cardiovascular model. The experimental setup, as shown in Figure 15, consisted of two parts. In the remote site, a silicone-based vascular phantom (EndoVascular Evaluator (EVE), FAIN-Biomedical Inc., Japan) was used. The slave end-effector actuated the guidewire and balloon catheter into the EVE model. A camera was mounted immediately beside the EVE model, in order to obtain visual feedback during the experimental process. In the local site, the physician navigated the vascular instruments through the master haptic interface to guide the vascular instruments from the femoral artery to several targets in the EVE model. The 5-F guiding catheter placement was performed manually through the brachial artery for arterial access. A 2.5 mm × 15 mm balloon catheter and a 0.014-inch guidewire were loaded into the roller module separately. The image information from the camera was presented on the computer monitor. The guidewire and balloon catheter were controlled by the master–slave robotic system to enter different vascular branches.

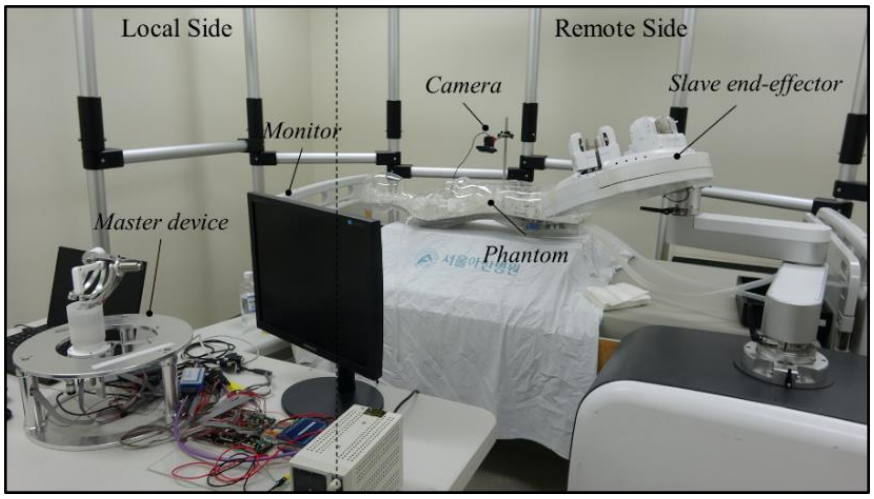

Figure 15. Phantom experimental setup for percutaneous coronary intervention procedure.

b) Experimental Results: Figure 16 shows that the guidewire and balloon catheter were located in the two targets. Figure 16 (a) shows that the guidewire was advanced and positioned at the first target, and Figure 16 (b) illustrates that the balloon catheter was advanced through the guidewire to the target point, and positioned fully at the first target. As shown in Figure 16 (c) ~ (d), the physician worked on the master device to operate the slave end-effector, to achieve simultaneous translational and rotational motions of the guidewire, and the guidewire was advanced to a new branch quickly and accurately. In Figure 16 (e) ~ (f), it can be observed that the guidewire advanced and reached the second target. Then, the balloon catheter was also advanced through the guidewire and positioned at the second target. The experiment confirmed that the guidewire and balloon catheter can be smoothly moved and precisely positioned using the proposed system. Figure 17 illustrates the translational and rotational motion trajectories of the guidewire and balloon catheter in the master and slave systems in the phantom experiment. In stage 1, the guidewire was inserted into the first target for translational motion, and in stage 2, the balloon catheter was inserted into the first target. Then, in stage 3, the guidewire was simultaneously advanced and rotated to move to the other branch, and it reached the second target. In stage 4, the balloon catheter was inserted into the second target.

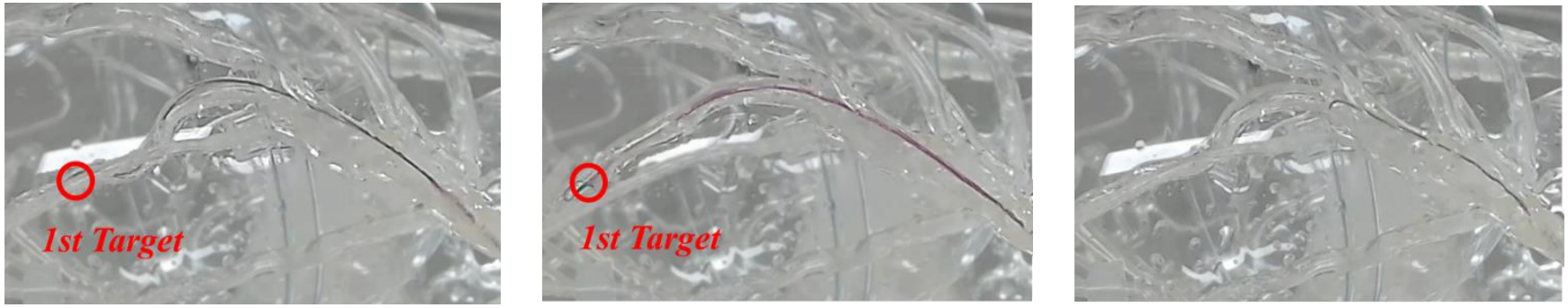

(**a**) (**b**) (**c**)

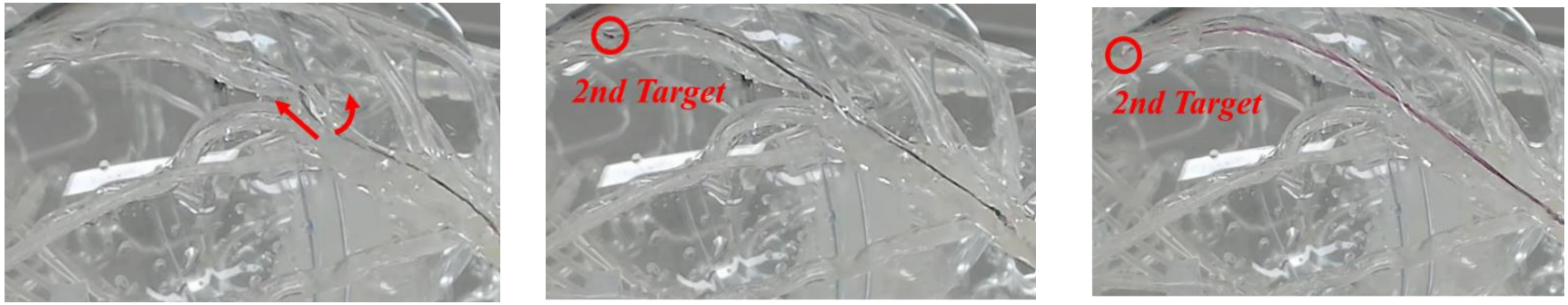

(**d**) (**e**) (**f**)

Figure 16. Two-dimensional views of the left coronary artery in the phantom. (a) Guidewire is positioned, (b) balloon catheter is positioned at the target, (c) guidewire is retracted, (d) guidewire is advanced, (e) it is positioned, (f) balloon catheter is positioned at the second target.

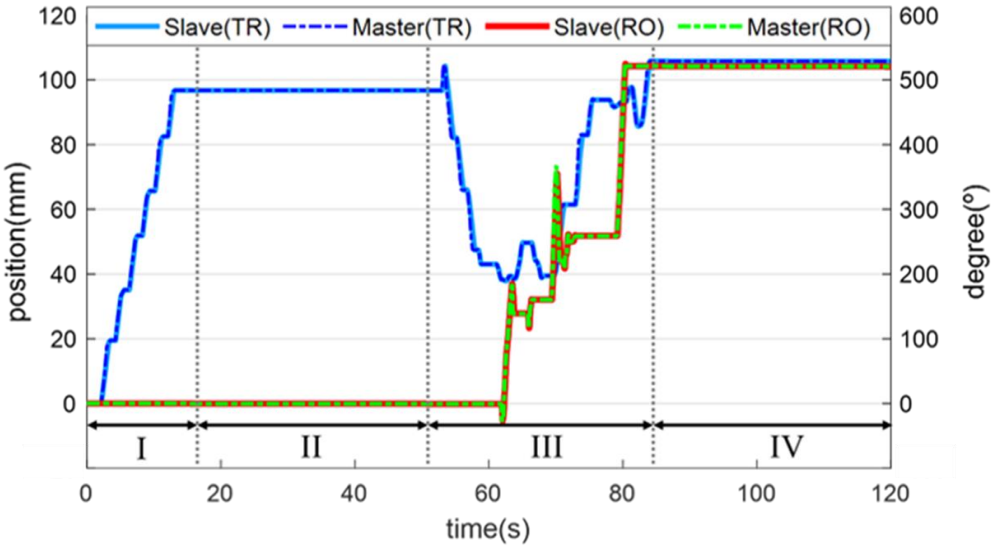

(**a**)

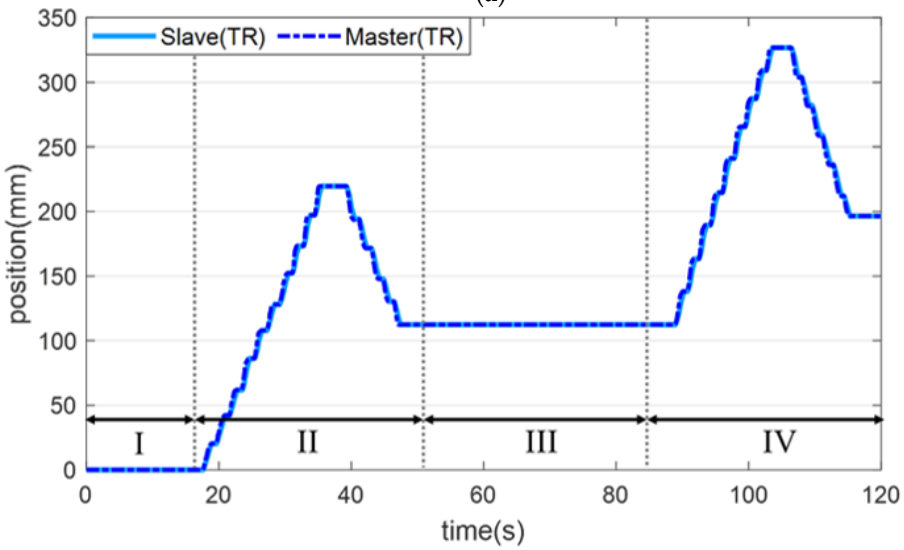

(**b**)

Figure 17. Translation and rotation information of the (a) guidewire and (b) balloon catheter when they are navigated to the target points.

3.2. In-vivo Test

Before the clinical trial, an experiment using a porcine model was performed to verify the functionality and safety of the proposed system.

a) Experimental Method: An animal experiment, using a porcine model, was performed to verify the proposed system's functionality and safety under an IACUC (Institutional Animal Care and Use Committee) approval of the Osong Medical Innovation Foundation, Republic of Korea (KBIO-IACUC-2019-105-1), as shown in Figure 18. The process of the experiment was as follows. First, the guiding catheter was manually inserted and engaged in the coronary ostium in the pig. Next, the slave robot was placed next to the bed and the end-effector was positioned close to the leg of the pig using a manual robot arm, and the master console was positioned outside the operating room. The physician operated the master haptic interface to remotely control the slave end-effector for translation and rotation of the guidewire under the guidance of an angiography image. The guidewire was inserted into two branches, and it reached the final target location using the robotic system. Finally, postoperative observation was conducted to confirm whether there was a complication.

(**a**) (**b**)

Figure 18. Setup of the animal experiment. (a) The slave robot beside the operation table and (b) the physician at the master console.

b) Experimental Results: The angiography images of each stage in the process of guidewire advancement are shown in Figure 19. The guidewire was advanced, and it reached the first branch point, as shown in Figure 19 (a). Then, the guidewire was withdrawn from the first branch by moving backward and rotating it, and it was advanced again to reach the second branch, as shown in Figure 19 (b). Finally, the guidewire was retracted and rotated again to exit from the second branch point, and then it was advanced to successfully reach the final target location, as shown in Figure 19 (c).

For postoperative observation, the physician manually withdrew the guidewire and then confirmed that there were no complications such as perforation or bleeding.

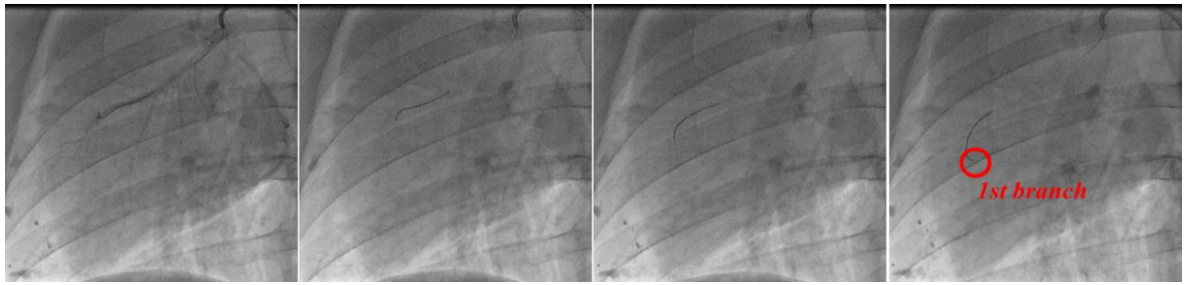

(**a**)

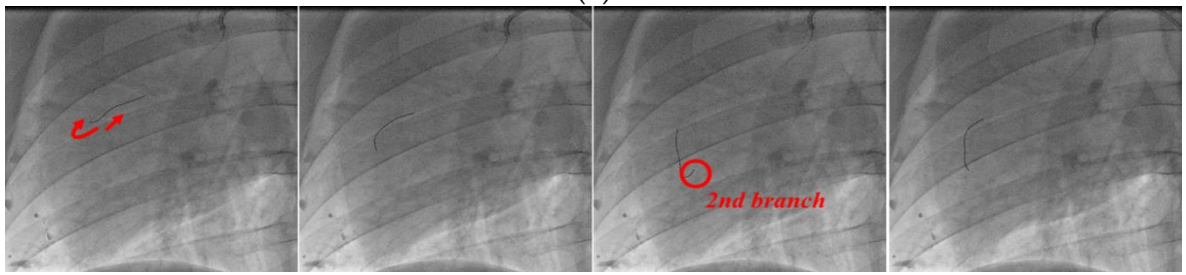

(**b**)

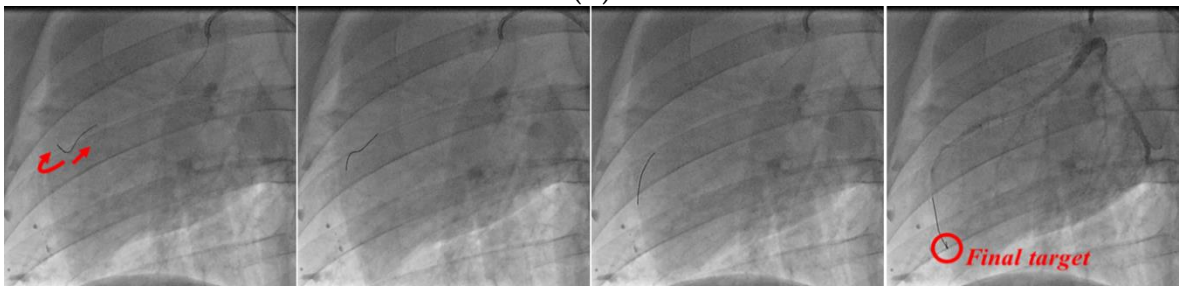

(**c**)

Figure 19. Angiographic views of the right coronary artery of the pig. Process of inserting guidewire into (a) first branch, (b) second branch, and (c) final target.

3.3. Clinical Trial

a) Experimental Method: A single-center, single-group clinical trial was conducted on two patients requiring coronary angiography at Asan Medical Center, Seoul, Republic of Korea (Asan Medical Center Institutional Review Board Registration Number: S2018-2377-0002), as shown in Figure 20. The clinical trial procedure was conducted as follows:

1) Setup of robot was prepared, such as sterile drapes and loading detachable sterilized rollers.

2) Arterial access and guiding catheter placement of coronary ostium were performed manually.

3) After the guiding catheter was located in the coronary artery completely, using the manual robot arm in the slave robot, the slave end-effector was positioned beside the bed on which the patient was lying, and the master console was located far from the patient. A guidewire was loaded by a tableside assistant into appropriate roller modules, which serves as the sterile interface between the slave end-effector and the patients.

4) The physician sat in front of the master console with a radiation-shielded wall and used the master haptic interface and touchscreen controls to advance, retract, rotate, and deploy the devices as required.

5) A guidewire was inserted into the target vessel site using a robotic system through a guiding catheter inserted manually.

6) When the guidewire was positioned at the desired location, coronary angiography was completed.

7) After 4 h of bed stability, patients were monitored for bleeding complications, and at 24 h after the procedure, patients were checked for the occurrence of an abnormal event/severe abnormal event.

b) Experimental Results: For efficacy evaluation, in the coronary angiography of the two subjects participating in this clinical trial, the guidewire was transferred to the target site of the

coronary artery (Subject I: “left anterior descending artery,” Subject II: “right coronary artery”) using the proposed master-slave robotic system without manual manipulation as shown in Figure 21. At this time, there was no damage or dissection of the distal intima (“Coronary artery dissection- The National Heart, Lung and Blood Institute classification” criteria, evaluated as Type A*). Accordingly, coronary angiography using the proposed master-slave robotic system of the two subjects registered in this clinical trial was evaluated as a “technological success”.

(**a**) (**b**)

Figure 20. Setup of the clinical trial. (a) The slave robot and the patients in the operation room are shown. (b) The physician is located in the corner of the angiography room with the master console, behind a radiation-shielded glass wall.

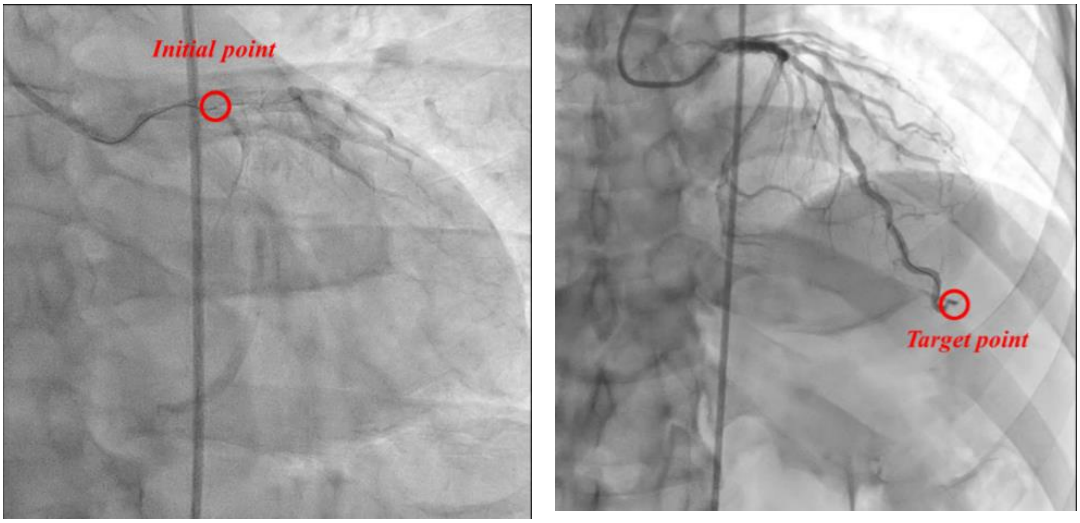

(**a**) (**b**)

21. Angiographic views of the left coronary artery of patient 1. (a) The guidewire was located at the entrance of coronary. (b) The guidewire was located at target point.

DISCUSSION

A master–slave robotic system with roller cartridge-based modules for robotic cardiovascular intervention has been developed for clinical application. Preliminary experiments were conducted to evaluate the performance of the roller cartridge-based modularized robotic system. Specific problems associated with the roller cartridges were adequately alleviated by compensation control and a force rendering method using the master haptic interface. Through the experiment using the phantom, we checked the functionality and safety of the master–slave robotic system. It was confirmed that no significant problems were identified in the master–slave system, and the positioning precision and accuracy of the guidewire and balloon catheter were also sufficiently high. It was also shown that the combination of translation, rotation, and their simultaneous motion enables vascular instruments to navigate to the desired location in the vascular branches. The in vivo animal experiment confirmed that navigating a guidewire in several branches worked smoothly as the physician manipulated the master haptic interface. In the clinical trial, the initial verification and validity of the prototype of the master–slave robotic system was confirmed by navigating the guidewire to the target location completely. Further in vivo tests should be performed to assess the clinical efficacy of the system.

Maor et al.[11] presented the limitations of an existing percutaneous coronary intervention (PCI) robot, such as the absence of tactile feedback and limited applicability to various complex vascular intervention procedures. The system presented in this study is similar to the Corpath system in its purpose and instrumentation motion. Although a haptic interface has been implemented in the master console, the utilization was only for haptic rendering. Further development and evaluation are needed and are underway to appropriately show the usefulness of the haptic interface that is designed to capture and interact with the physician's positional and rotational motion via the 6-DOF mechanism. The methods for the repulsive force measurement and direct force feedback need further study. There is a need for a method to solve various nonlinear factors caused by interactions between surgical environmental factors, instruments, and robots. In future work, the model of a force feedback for telepresence, a control with higher level of autonomy, robotic procedures to implement safer tasks in less time, and a new design of a robotic system suitable for more complex PCI should be considered.

CONCLUSION

The robotic system proposed in this study was confirmed to help the physician perform vascular intervention successfully and efficiently though experiments. The slave end-effector could control the translational and rotational motions of the vascular instruments using a roller-cartridge-based modularized robotic system. The development of the active clamping mechanism is convenient for gripping and releasing vascular instruments and appropriate for applying a clamping force for vascular instruments of different sizes. Several experiments were conducted to validate the master-slave robotic system.

REFERENCE

1. Per Bergman, Steven J. Blacker, Nicholas Kottenstette, Omid Saber, Saeed Sokhanvar, 20 - Robotic-Assisted Percutaneous Coronary Intervention, Editor(s): Mohammad H. Abedin-Nasab, Handbook of Robotic and Image-Guided Surgery, Elsevier, 2020, Pages 341-362.

2. Mohapatra A, Greenberg RK, Mastracci TM, Eagleton MJ, Thornsberry B. Radiation exposure to operating room personnel and patients during endovascular procedures. J Vasc Surg. 2013 Sep;58(3):702-9.

3. Klein LW, Miller DL, Balter S, Laskey W, Naito N, Haines D, Ross A, Mauro MA, Goldstein JA. Occupational health hazards in the interventional laboratory: Time for a safer environment. Catheter Cardiovasc Interv. 2018 Jan 4.

4. Rafii-Tari H, Payne CJ, Yang GZ. Current and emerging robot-assisted endovascular catheterization technologies: a review. Ann Biomed Eng. 2014 Apr;42(4):697-715.

5. Costa MA, Angiolillo DJ, Tannenbaum M, Driesman M, Chu A, Patterson J, Kuehl W, Battaglia J, Dabbons S, Shamoon F, Flieshman B, Niederman A, Bass TA; STLLR Investigators. Impact of stent deployment procedural factors on long-term effectiveness and safety of sirolimus-eluting stents (final results of the multicenter prospective STLLR trial). Am J Cardiol. 2008 Jun 15;101(12):1704-11.

6. Carrozza JP Jr. Robotic-assisted percutaneous coronary intervention-filling an unmet need. J Cardiovasc Transl Res. 2012 Feb;5(1):62-6.

7. Mahmud E, Dominguez A, Bahadorani J. First-in-human robotic percutaneous coronary intervention for unprotected left main stenosis. Catheter Cardiovasc Interv. 2016 Oct;88(4):565-570.

8. Omisore OM, Han SP, Ren LX, Wang GS, Ou FL, Li H, Wang L. Towards Characterization and Adaptive Compensation of Backlash in a Novel Robotic Catheter System for Cardiovascular Interventions. IEEE Trans Biomed Circuits Syst. 2018 Aug;12(4):824-838.

9. Mangels DR, Giri J, Hirshfeld J, Wilensky RL. Robotic-assisted percutaneous coronary intervention. Catheter Cardiovasc Interv. 2017 Nov 15;90(6):948-955.

10. Walters D, Omran J, Patel M, Reeves R, Ang L, Mahmud E. Robotic-Assisted Percutaneous Coronary Intervention: Concept, Data, and Clinical Application. Interv Cardiol Clin. 2019 Apr;8(2):149-159.

11. Maor E, Eleid MF, Gulati R, Lerman A, Sandhu GS. Current and Future Use of Robotic Devices to Perform Percutaneous Coronary Interventions: A Review. J Am Heart Assoc. 2017 Jul 24;6(7).

12. Weisz G, Metzger DC, Caputo RP, Delgado JA, Marshall JJ, Vetrovec GW, Reisman M, Waksman R, Granada JF, Novack V, Moses JW, Carrozza JP. Safety and feasibility of robotic percutaneous coronary intervention: PRECISE (Percutaneous Robotically-Enhanced Coronary Intervention) Study. J Am Coll Cardiol. 2013 Apr 16;61(15):1596-600.

13. Smilowitz NR, et al. Robotic-enhanced PCI compared to the traditional manual approach. J Invasive Cardiol 2014;26(7):318-21.

14. Mahmud E, Pourdjabbar A, Ang L, Behnamfar O, Patel MP, Reeves RR. Robotic technology in interventional cardiology: Current status and future perspectives. Catheter Cardiovasc Interv. 2017 Nov 15;90(6):956-962.

15. Riga CV, Bicknell CD, Rolls A, Cheshire NJ, Hamady MS. Robot-assisted fenestrated endovascular aneurysm repair (FEVAR) using the Magellan system. J Vasc Interv Radiol. 2013 Feb;24(2):191-6.

16. Rolls AE, Riga CV, Bicknell CD, Regan L, Cheshire NJ, Hamady MS. Robot-assisted uterine artery embolization: a first-in-woman safety evaluation of the Magellan System. J Vasc Interv Radiol. 2014 Dec;25(12):1841-8.

17. Riga C, Bicknell C, Hamady MS, Cheshire NJ. Robotically-steerable catheters and their role in the visceral aortic segment. J Cardiovasc Surg (Torino). 2011 Jun;52(3):353-62.

18. Weisz, G., Metzger, D.C., Caputo, R.P., Delgado, J.A., Marshall, J.J., Vetrovec, G.W. et al, J.P. Safety and feasibility of robotic percutaneous coronary intervention: PRECISE (Percutaneous Robotically-Enhanced Coronary Intervention) Study. J. Am. Coll Cardiol. 2013, 61, 1596–1600.

19. Hooshiar A, Najarian S, Dargahi J. Haptic Telerobotic Cardiovascular Intervention: A Review of Approaches, Methods, and Future Perspectives. IEEE Rev Biomed Eng. 2020;13:32-50.

20. Thakur Y, Bax JS, Holdsworth DW, Drangova M. Design and performance evaluation of a remote catheter navigation system. IEEE Trans Biomed Eng. 2009 Jul;56(7):1901-8.

21. Thakur Y, Holdsworth DW, Drangova M. Characterization of catheter dynamics during percutaneous transluminal catheter procedures. IEEE Trans Biomed Eng. 2009 Aug;56(8):2140-3.

22. Cha HJ, Yi BJ, Won JY. An assembly-type master-slave catheter and guidewire driving system for vascular intervention. Proc Inst Mech Eng H. 2017 Jan;231(1):69-79.

23. Choi J, Park S, Kim Y-H, Moon Y, Choi J. A Vascular Intervention Assist Device Using Bi-Motional Roller Cartridge Structure and Clinical Evaluation. Biosensors. 2021; 11(9):329.

24. Z. Feng, G. Bian, X. Xie, Z. Hou and Jian-Long Hao. Design and evaluation of a bio-inspired robotic hand for percutaneous coronary intervention. IEEE International Conference on Robotics and Automation (ICRA), 2015, pp. 5338-5343.

25. Srimathveeravalli G, Kesavadas T, Li X. Design and fabrication of a robotic mechanism for remote steering and positioning of interventional devices. Int J Med Robot. 2010 Jun;6(2):160-70.

26. C. Meng, S. Guan, S. Sun, Y. Liu, T. Wang. A novel catheter operating robot for vascular interventional surgery. IEEE Workshop on Advanced Robotics and its Social Impacts (ARSO), 2016, pp. 304-309.

27. Moon, Y., Hu, Z., Won, J. et al. Novel Design of Master Manipulator for Robotic Catheter System. Int. J. Control Autom. Syst. 16, 2924–2934 (2018).

28. Merlet, Jean-Pierre. Direct kinematics of planar parallel manipulators. Proceedings - IEEE International Conference on Robotics and Automation. 1996.

29. Gosselin, C., and Angeles, J. The Optimum Kinematic Design of a Planar Three-Degree-of-Freedom Parallel Manipulator. ASME. J. Mech., Trans., and Automation. March 1988; 110(1): 35–41.

30. V.H. Arakelian, M.R. Smith. Design of planar 3-DOF 3-RRR reactionless parallel manipulators. Mechatronics, Vol 18, Issue 10, 2008.

31. Ouafae Hamdoun, Larbi El Bakkali, Fatima Zahra Baghli, Analysis and Optimum Kinematic Design of a Parallel Robot, Procedia Engineering, Vol 181, 2017, Pages 214-220.

KOREAN ABSTRACT

혈관 중재 시술이란 혈관 조영장비 등의 영상장비를 통해 혈관 속을 관찰하면서 가는 도관(카테터, catheter) 들어갈 수 있는 작은 구멍을 통해 병변에 도달하여 치료하는 방법이다. 본 시술은 시술 안전성이 높고 환자의 예후가 우수할 뿐만 아니라 통증과 흉터를 최소화하는 등 여러 장점이 있다.

방사선 피폭 등의 문제점을 해결하고 중재시술의 결과를 더욱 향상시키기 위해서는 정밀하고 정확한 시술을 짧은 시간 내에 가능하게 할 수 있는 의료 기기의 개발이 필수적이며, 다양한 형태의 로봇 시스템 연구가 진행되고 있다.

이미 상용화된 로봇 시스템은 사용할 수 있는 시술 도구가 제한되어 있으며, 또한 범용성 마스터 장치를 이용하기 때문에, 카테터를 운용할 때, 시술자에게 정교한 햅틱 피드백을 제공할 수 없다는 문제점이 있다.

본 연구는 이러한 필요성을 바탕으로 다양한 크기의 시술 도구를 사용할 수 있도록, 능동 클램핑 메커니즘을 가진 슬레이브 엔드이펙터와 햅틱 기능을 구현할 수 있도록 마스터 장치를 가진 원격 제어 가능한 로봇 시스템을 제안한다.

슬레이브 엔드이펙터는 시술 도구를 전후진, 회전시켜 제어하고 시술도구와 직접 접촉하는 부분은 1 회용으로 사용할 수 있도록 해야 한다. 이러한 사항을 고려하여 롤러 메커니즘을 이용한 슬레이브 엔드이펙터를 제안한다. 또한, 이를 원격으로 제어하기 위한 마스터 장치를 제안한다. 마스터 장치는 6 자유도를 가지고 시술자가 슬레이브 엔드이펙터의 상황 또는 입력 모션에 대해 좀 더 편리하게 느낄 수 있도록 햅틱 기능을 구현한다. 슬레이브 엔드이펙터의 제어 개선과 햅틱 렌더링에 관한 보상 방법을 제시하고 평가하고자 한다.

마지막으로 슬레이브-마스터 로봇을 통합하여 다양한 팬텀 및 동물 실험을 통해 시스템의 성능을 입증하고. 임상 시험을 통해 본 시스템의 임상적 유효성을 평가하고자 한다.